

Theory of Spin Fluctuation-Induced Superconductivity Based on a d - p Model II —Superconducting State—

Tetsuya Takimoto *and Tôru Moriya¹

Electrotechnical Laboratory, Tsukuba, Ibaraki 305

¹*Department of Physics, Faculty of Science and Technology, Science University of Tokyo, Noda 278*

(May , 1998)

Abstract

The superconducting state of a two-dimensional d - p model is studied from the spin fluctuation point of view by using a strong coupling theory. The fluctuation exchange (FLEX) approximation is employed to calculate the spin fluctuations and the superconducting gap functions self-consistently in the optimal- and over-doped regions of hole concentration. The gap function has a symmetry of $d_{x^2-y^2}$ type and develops below the transition temperature T_c more rapidly than in the BCS model. Its saturation value at the maximum is about $10k_B T_c$. When the spin fluctuation-induced superconductivity is well stabilized at low temperatures in the optimal regime, the imaginary part of the antiferromagnetic spin susceptibility shows a very sharp resonance peak reminiscent of the 41 meV peak observed in the neutron scattering experiment on $\text{YBa}_2\text{Cu}_3\text{O}_7$. The one-particle spectral density around $\mathbf{k} = (\pi, 0)$ shows sharp quasi-particle peaks followed by dip and hump structures bearing resemblance to the features observed in the angle-resolved photoemission experiment. With increasing doping concentration these features gradually disappear.

1 Introduction

Among a number of mechanisms proposed for the high temperature superconductivity since its discovery in 1986 the spin fluctuation mechanism has continued to be one of the most promising mechanisms. [1, 2, 3, 4, 5, 6, 7] Following systematic studies based on the parameterized spin fluctuation theory, more quantitative studies were carried out by using the Hubbard model [8, 9, 10, 11, 12, 13, 14] and the d - p model [15, 16, 17, 18] within the so-called fluctuation exchange (FLEX) approximation.

In a previous article [18] (hereafter referred to as I) we have developed a strong coupling theory of spin fluctuation-induced superconductivity on a microscopic basis by using a two-dimensional d - p model and applied it to interpret high T_c cuprates. We adopted the fluctuation exchange (FLEX) approximation in calculating the transition temperature T_c , the dynamical susceptibility, nuclear spin-lattice relaxation rate, and the one-particle spectral density above T_c . The results compared rather well with the experimental results on cuprates in the optimal- and the over-doped regimes.

In the present article we extend the calculation to the superconducting state below T_c . By using the d - p model with the same parameter values as in I, we solve the non-linear Dyson-Gor'kov equations numerically and calculate various physical quantities; the energy gap function, the one-particle density of states, dynamical susceptibility and the one-particle spectral density. The results of calculation are discussed in comparison with the existing experimental results, particularly the resonance peak at 41 meV, observed in the neutron scattering experiment on $\text{YBa}_2\text{Cu}_3\text{O}_7$ [19, 20, 21, 22, 23] and the observed angle-resolved photoemission spectrum (ARPES), showing a resolution-limited quasi-particle peak followed by a dip and a hump structure around the $(\pi, 0)$ point. [24, 25, 26, 27]

In what follows we first summarize the model and the formalism we use here in § 2. In § 3 the results of calculation are presented and discussed in comparison with the existing experimental results. Finally, § 4 is devoted for summary of conclusions and general discussion.

*Japan Science and Technology Corporation, Domestic Research Fellow.

2 Model and Approach

The model we use here is the same as in I; the d - p model consisting of the $d_{x^2-y^2}$ orbitals of copper atoms and the p_σ (p_x and p_y) orbitals of oxygen atoms in the CuO_2 plane of cuprates. The energy levels of these orbitals are ϵ_d and ϵ_p , respectively, and the transfer matrix elements are considered only between the neighboring d and p orbitals (t_{dp}) and between the neighboring p_x and p_y orbitals (t_{pp}) where the parities of both the $d_{x^2-y^2}$ orbital and the p_σ (p_x and p_y) orbitals are taken into account. For brevity, the Hubbard type electron-electron interaction U is considered only within a d orbital, and the other effects are assumed to be contained in ϵ_d and ϵ_p as the Hartree potentials. The Hamiltonian may be written as follows:

$$H = H_0 + H_1, \quad (1)$$

$$H_0 = \sum_{\mathbf{k}, \sigma} [\epsilon_d d_{\mathbf{k}\sigma}^\dagger d_{\mathbf{k}\sigma} + \sum_{m=1}^2 \{ \{\epsilon_p - (-1)^m t_p(\mathbf{k})\} p_{m\mathbf{k}\sigma}^\dagger p_{m\mathbf{k}\sigma} + \{it_m(\mathbf{k}) d_{\mathbf{k}\sigma}^\dagger p_{m\mathbf{k}\sigma} + h.c.\} \}], \quad (2)$$

with

$$\begin{aligned} t_m(\mathbf{k}) &= \sqrt{2} t_{dp} [\sin(k_x a/2) - (-1)^m \sin(k_y a/2)], \\ t_p(\mathbf{k}) &= 4 t_{pp} \sin(k_x a/2) \sin(k_y a/2), \end{aligned} \quad (3)$$

and

$$\begin{aligned} H_1 &= U \sum_j n_{dj\uparrow} n_{dj\downarrow} \\ &= \frac{U}{N_0} \sum_{\mathbf{q}} \sum_{\mathbf{k}} \sum_{\mathbf{k}'} d_{\mathbf{k}+\mathbf{q}\uparrow}^\dagger d_{\mathbf{k}'-\mathbf{q}\downarrow}^\dagger d_{\mathbf{k}'\downarrow} d_{\mathbf{k}\uparrow}, \end{aligned} \quad (4)$$

where $d_{\mathbf{k}\sigma}$ and $p_{m\mathbf{k}\sigma}$ ($m = 1, 2$) are the Fourier transforms of the annihilation operators for the electrons in the d and $p_m = \frac{1}{\sqrt{2}}[p_x - (-1)^m p_y]$ orbitals, respectively, and N_0 is the number of atoms in the crystal.

We denote the diagonalized expression for H_0 as follows:

$$H_0 = \sum_{\mathbf{k}, \sigma} \sum_{m=1}^3 E_{m\mathbf{k}\sigma} a_{m\mathbf{k}\sigma}^\dagger a_{m\mathbf{k}\sigma}, \quad (5)$$

$$\begin{bmatrix} a_{1\mathbf{k}\sigma} \\ a_{2\mathbf{k}\sigma} \\ a_{3\mathbf{k}\sigma} \end{bmatrix} = \begin{bmatrix} \beta_{11\mathbf{k}} & \beta_{12\mathbf{k}} & \beta_{13\mathbf{k}} \\ \beta_{21\mathbf{k}} & \beta_{22\mathbf{k}} & \beta_{23\mathbf{k}} \\ \beta_{31\mathbf{k}} & \beta_{32\mathbf{k}} & \beta_{33\mathbf{k}} \end{bmatrix} \begin{bmatrix} d_{\mathbf{k}\sigma} \\ p_{1\mathbf{k}\sigma} \\ p_{2\mathbf{k}\sigma} \end{bmatrix}. \quad (6)$$

Then the Green's functions for the non-interacting system is given by

$$G_{\lambda\nu}^{(0)}(\mathbf{k}, i\omega_n) = \sum_{m=1}^3 \beta_{m\lambda\mathbf{k}}^* \beta_{m\nu\mathbf{k}} \frac{1}{i\omega_n + \mu - E_{m\mathbf{k}\sigma}}, \quad (7)$$

where $\lambda(\nu)=1,2$ and 3 stand for d , p_1 and p_2 orbitals, respectively, $\omega_n = (2n+1)\pi T$ is the Fermion Matsubara frequency and μ is the chemical potential. $E_{m\mathbf{k}\sigma}$ and $\beta_{m\lambda\mathbf{k}}$ can be calculated from ϵ_d , ϵ_p , t_{dp} and t_{pp} . In what follows we express all the energies in units of t_{dp} .

The Dyson-Gor'kov equations for the Green's functions $G_{\lambda\nu}(\mathbf{k}, i\omega_n)$ and the anomalous Green's functions $F_{\lambda\nu}^\dagger(\mathbf{k}, i\omega_n)$ are given by

$$G_{\lambda\nu}(\mathbf{k}, i\omega_n) = G_{\lambda\nu}^{(0)}(\mathbf{k}, i\omega_n) + G_{\lambda 1}^{(0)}(\mathbf{k}, i\omega_n) [\Sigma^{(1)}(\mathbf{k}, i\omega_n) G_{1\nu}(\mathbf{k}, i\omega_n) - \Sigma^{(2)}(\mathbf{k}, i\omega_n) F_{1\nu}^\dagger(\mathbf{k}, i\omega_n)], \quad (8)$$

$$F_{\lambda\nu}^\dagger(\mathbf{k}, i\omega_n) = G_{\lambda 1}^{(0)}(-\mathbf{k}, -i\omega_n) [\Sigma^{(1)}(-\mathbf{k}, -i\omega_n) F_{1\nu}^\dagger(\mathbf{k}, i\omega_n) + \Sigma^{(2)}(-\mathbf{k}, -i\omega_n) G_{1\nu}(\mathbf{k}, i\omega_n)], \quad (9)$$

where the self-energies due to the spin and charge fluctuations are given within the FLEX approximation as follows:

$$\Sigma^{(1)}(\mathbf{k}, i\omega_n) = \frac{T}{N_0} \sum_{\mathbf{q}, m} V_{\text{eff}}(\mathbf{q}, i\Omega_m) G_{dd}(\mathbf{k} - \mathbf{q}, i\omega_n - i\Omega_m), \quad (10)$$

$$\Sigma^{(2)}(\mathbf{k}, i\omega_n) = -\frac{T}{N_0} \sum_{\mathbf{q}, m} V_{\text{sing}}(\mathbf{q}, i\Omega_m) F_{dd}(\mathbf{k} - \mathbf{q}, i\omega_n - i\Omega_m), \quad (11)$$

with

$$V_{\text{eff}}(\mathbf{q}, i\Omega_m) = U + U^2 \left[\frac{3}{2} \chi_d^s(\mathbf{q}, i\Omega_m) + \frac{1}{2} \chi_d^c(\mathbf{q}, i\Omega_m) - \frac{1}{2} \{ \bar{\chi}_d^s(\mathbf{q}, i\Omega_m) + \bar{\chi}_d^c(\mathbf{q}, i\Omega_m) \} \right], \quad (12)$$

$$V_{\text{sing}}(\mathbf{q}, i\Omega_m) = U + U^2 \left[\frac{3}{2} \chi_d^s(\mathbf{q}, i\Omega_m) - \frac{1}{2} \chi_d^c(\mathbf{q}, i\Omega_m) - \frac{1}{2} \{ \bar{\chi}_d^s(\mathbf{q}, i\Omega_m) - \bar{\chi}_d^c(\mathbf{q}, i\Omega_m) \} \right], \quad (13)$$

and

$$\chi_d^s(\mathbf{q}, i\Omega_m) = \frac{\bar{\chi}_d^s(\mathbf{q}, i\Omega_m)}{1 - U \bar{\chi}_d^s(\mathbf{q}, i\Omega_m)}, \quad \chi_d^c(\mathbf{q}, i\Omega_m) = \frac{\bar{\chi}_d^c(\mathbf{q}, i\Omega_m)}{1 + U \bar{\chi}_d^c(\mathbf{q}, i\Omega_m)}, \quad (14)$$

$$\bar{\chi}_d^s(\mathbf{q}, i\Omega_m) = -\frac{T}{N_0} \sum_{\mathbf{k}, n} [G_{dd}(\mathbf{k} + \mathbf{q}, i\omega_n + i\Omega_m) G_{dd}(\mathbf{k}, i\omega_n) + F_{dd}(\mathbf{k} + \mathbf{q}, i\omega_n + i\Omega_m) F_{dd}(\mathbf{k}, i\omega_n)], \quad (15)$$

$$\bar{\chi}_d^c(\mathbf{q}, i\Omega_m) = -\frac{T}{N_0} \sum_{\mathbf{k}, n} [G_{dd}(\mathbf{k} + \mathbf{q}, i\omega_n + i\Omega_m) G_{dd}(\mathbf{k}, i\omega_n) - F_{dd}(\mathbf{k} + \mathbf{q}, i\omega_n + i\Omega_m) F_{dd}(\mathbf{k}, i\omega_n)], \quad (16)$$

where $\Omega_m = 2m\pi T$ is the Bose Matsubara frequency.

The number of d - and p -electrons per site (respectively, n_d and n_p) and the doping concentration δ are given by

$$n_d = 2 \lim_{\tau \rightarrow +0} \frac{T}{N_0} \sum_{\mathbf{k}, n} e^{i\omega_n \tau} G_{dd}(\mathbf{k}, i\omega_n),$$

$$n_p = \lim_{\tau \rightarrow +0} \frac{T}{N_0} \sum_{\mathbf{k}, n} e^{i\omega_n \tau} [G_{22}(\mathbf{k}, i\omega_n) + G_{33}(\mathbf{k}, i\omega_n)],$$

$$\delta = 5 - (n_d + 2n_p),$$

where the "half-filled" state corresponds to $n_d + 2n_p = 5$.

For the purpose of calculating T_c we linearize eqs.(8) and (9) with respect to $F_{dd}^\dagger(\mathbf{k}, i\omega_n)$ or $\Sigma^{(2)}(\mathbf{k}, i\omega_n)$ as follows:

$$\frac{1}{G_{dd}(\mathbf{k}, i\omega_n)} = \frac{1}{G_{dd}^{(0)}(\mathbf{k}, i\omega_n)} - \Sigma^{(1)}(\mathbf{k}, i\omega_n), \quad (17)$$

$$F_{dd}^\dagger(\mathbf{k}, i\omega_n) = G_{dd}(-\mathbf{k}, -i\omega_n) \Sigma^{(2)}(-\mathbf{k}, -i\omega_n) G_{dd}(\mathbf{k}, i\omega_n). \quad (18)$$

The normal Green's functions are now calculated self-consistently from eqs.(10), (12), (14) and (17). The critical temperature for the superconductivity is determined as the temperature below which the linearized equation for $\Sigma^{(2)}(\mathbf{k}, i\omega_n)$ has a non-trivial solution. The linearized equation is given by

$$\Sigma^{(2)}(\mathbf{k}, i\omega_n) = -\frac{T}{N_0} \sum_{\mathbf{p}, m} [V_{\text{sing}}(\mathbf{k} - \mathbf{p}, i\omega_n - i\omega_m) |G_{dd}(\mathbf{p}, i\omega_m)|^2]_{F_{dd} \rightarrow 0} \Sigma^{(2)}(\mathbf{p}, i\omega_m). \quad (19)$$

T_c is thus obtained by solving this eigenvalue problem, eq.(19); T_c is the temperature where the maximum eigenvalue becomes unity. The superconducting order parameter has the same symmetry as $\Sigma^{(2)}(\mathbf{k}, i\omega_n)$.

Below T_c we need to solve the nonlinear equations (from (7) to (16)) self-consistently. From the solution we calculate the one-particle spectra $A(\mathbf{k}, \omega)$ and the transverse dynamical spin susceptibility $\chi^{-+}(\mathbf{q}, \omega)$ by analytically continuing $G_{dd}(\mathbf{k}, i\omega_n)$ and $\chi_d^s(\mathbf{q}, i\Omega_m)$ from the imaginary-axis to the real-axis. The density of states $\rho(\omega)$ and the local spin susceptibility $\chi(\omega)$ are given as follows:

$$\rho(\omega) = \frac{1}{N_0} \sum_{\mathbf{k}} A(\mathbf{k}, \omega), \quad (20)$$

$$A(\mathbf{k}, \omega) = -\frac{1}{\pi} \text{Im} [G_{dd}(\mathbf{k}, \omega + i\eta) + G_{22}(\mathbf{k}, \omega + i\eta) + G_{33}(\mathbf{k}, \omega + i\eta)], \quad (21)$$

$$\text{Im} \chi(\omega) = \frac{1}{N_0} \sum_{\mathbf{q}} \text{Im} \chi^{-+}(\mathbf{q}, \omega), \quad \chi^{-+}(\mathbf{q}, \omega) = \chi_d^s(\mathbf{q}, \omega + i\eta), \quad (\eta \rightarrow +0). \quad (22)$$

Table 1: Parameter values for the d - p model and the calculated transition temperature T_c in units of t_{dp} for various doping concentrations.

$\epsilon_p - \mu$	n_d	n_p	$(2 - n_d)/(4 - 2n_p)$	δ	T_c
-2.600	1.314	1.799	1.703	0.0890	0.006621
-2.575	1.308	1.794	1.683	0.1029	0.006597
-2.550	1.302	1.790	1.663	0.1170	0.006475
-2.500	1.291	1.782	1.624	0.1451	0.006015
-2.450	1.280	1.773	1.585	0.1738	0.005351
-2.400	1.269	1.764	1.547	0.2037	0.004529

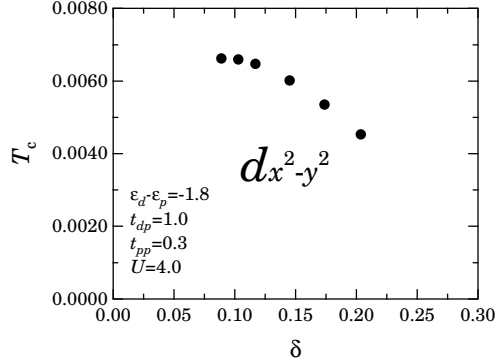


Fig. 1. Calculated values of T_c for various doping concentrations.

We define the gap functions in the following conventional way:

$$\Delta(\mathbf{k}, \omega) = \frac{\Sigma^{(2)}(\mathbf{k}, \omega + i\eta)}{Z(\mathbf{k}, \omega)}, \quad (23)$$

$$\omega Z(\mathbf{k}, \omega) = \omega - \frac{1}{2}[\Sigma^{(1)}(\mathbf{k}, \omega + i\eta) - \Sigma^{(1)}(\mathbf{k}, -\omega - i\eta)]. \quad (24)$$

3 Results of Calculation

3.1 Some details of numerical calculations.

To study the superconducting state, we first calculate the superconducting transition temperature T_c . For this purpose we calculate the kernel of the eigenvalue equation (19) at a fixed temperature, solving eqs. (10) and (12-17) for $\chi_d^s(\mathbf{q}, i\Omega_m)$, $\chi_d^c(\mathbf{q}, i\Omega_m)$ and $G_{dd}(\mathbf{k}, i\omega_n)$ self-consistently. Then, using the results of this calculation, we solve the eigenvalue problem. If eq. (19) do not have a non-trivial solution at a given temperature, we carry out the same calculation at a slightly decreased temperature. We repeat this routine until a error for T_c attains 10^{-6} . Below T_c , we calculate $\chi_d^s(\mathbf{q}, i\Omega_m)$, $\chi_d^c(\mathbf{q}, i\Omega_m)$, $G_{dd}(\mathbf{k}, i\omega_n)$ and $F_{dd}(\mathbf{k}, i\omega_n)$ by solving the non-linear equations (7) to (16), self-consistently.

All the sums involved in the self-consistent equations are carried out by using fast Fourier transforms (FFT) with the 64×64 meshes in the \mathbf{k} -space and the Matsubara frequency sum up to $|\omega_n| \approx 25|t_{dp}|$. The solution is obtained by iteration until the self-consistency condition is satisfied within the following accuracy:

$$\frac{|\Sigma_r^{(m)}(\mathbf{k}, i\omega_n) - \Sigma_{r-1}^{(m)}(\mathbf{k}, i\omega_n)|}{|\Sigma_r^{(m)}(\mathbf{k}, i\omega_n)|} < 10^{-6} \quad m = 1, 2. \quad (25)$$

The analytical continuations to the real frequency axis are carried out by using Padé approximants.

We need to take special care in evaluating $\rho(\omega)$ and $\text{Im}\chi(\omega)$ because of the size-effect due to the striking reduction of the quasi-particle damping in the superconducting state; after substituting the \mathbf{k} -summations

for $G_{dd}(\mathbf{k}, i\omega_n)$ or $\chi_d^s(\mathbf{q}, i\Omega_m)$ with numerical integrations by using the spline interpolation method, the Padé approximants are calculated.

Now, for the actual calculations, we choose the same parameter values as in I, $t_{pp} = 0.3$, $\epsilon_d - \epsilon_p = -1.8$, $U = 4$, in units of t_{dp} .

3.2 Transition temperature.

Although the present calculation has a better accuracy than the previous one, the results as shown in Table I and Fig. 1 are only slightly different from those in I. The calculated value of T_c and its doping concentration dependence are reasonable in the optimal and over-doped regimes while the observed reduction of T_c with decreasing doping concentration in the under-doped regime is hard to reproduce. The pairing symmetry of the calculated state is always of $d_{x^2-y^2}$. Thus it seems appropriate to confine ourselves in what follows to the superconducting state of this symmetry.

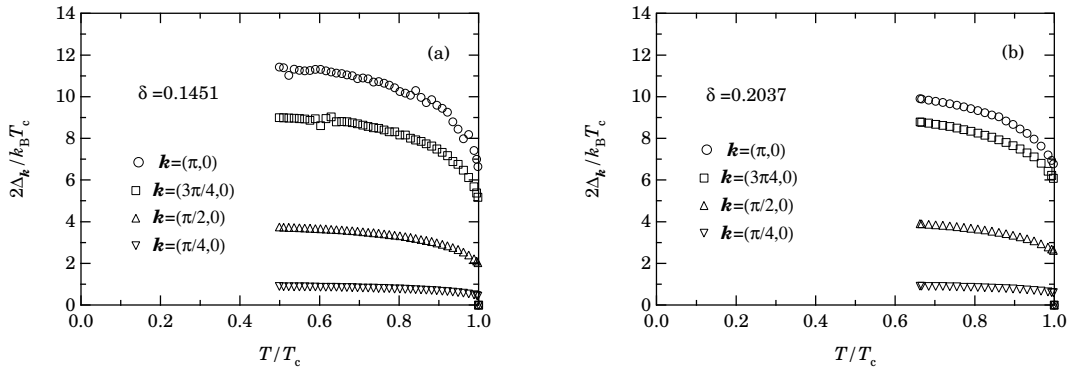


Fig. 2. Temperature dependence of $2\Delta_{\mathbf{k}}/k_B T_c$ for $\mathbf{k} = (\pi, 0)$, $(3\pi/4, 0)$, $(\pi/2, 0)$ and $(\pi/4, 0)$. (a) $\delta = 0.1451$, (b) $\delta = 0.2037$.

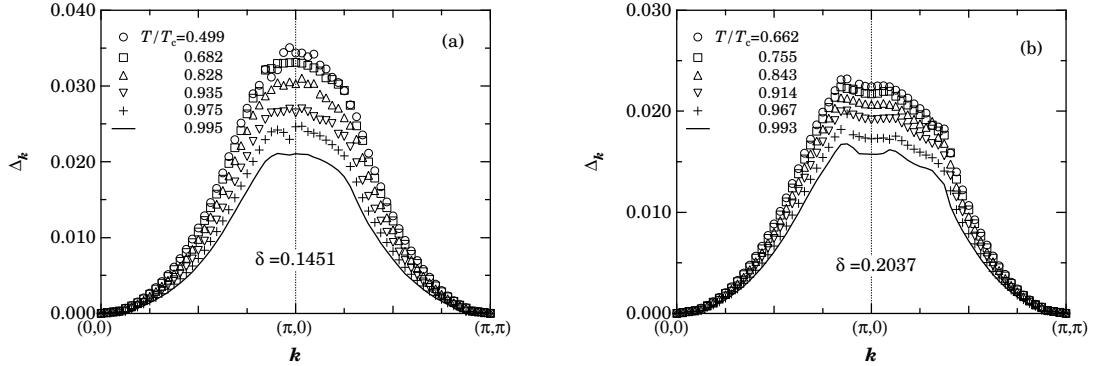


Fig. 3. Anisotropy of the gap function at various temperatures. (a) $\delta = 0.1451$, (b) $\delta = 0.2037$.

3.3 Gap function.

We calculate the gap function as defined conventionally in the Éliashberg theory; $\Delta_{\mathbf{k}} = \Delta(\mathbf{k}, \Delta_{\mathbf{k}})$. Fig. 2(a) shows the temperature dependence of $2\Delta_{\mathbf{k}}/k_B T_c$ for $\mathbf{k} = (\pi, 0)$, $(3\pi/4, 0)$, $(\pi/2, 0)$ and $(\pi/4, 0)$ for $\delta = 0.1451$ and Fig. 2(b) shows the corresponding results for $\delta = 0.2037$. We find that the superconducting gap develops more rapidly than in the BCS model. The maximum gap at $\mathbf{k} = (\pi, 0)$ saturates to a low temperature value

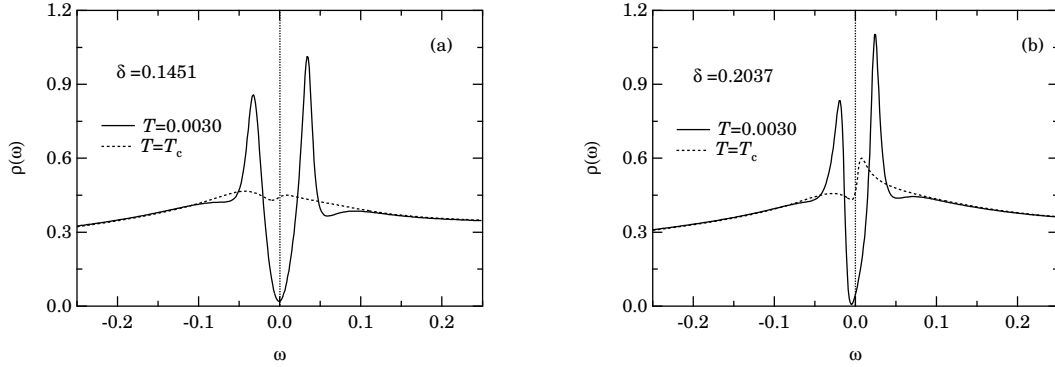


Fig. 4. One particle density of states. (a) $\delta = 0.1451$, (b) $\delta = 0.2037$.

of around $10k_B T_c$. We next show in Figs. 3(a) and 3(b) the \mathbf{k} -dependence of $\Delta_{\mathbf{k}}$ at varying temperatures for $\delta = 0.1451$ and $\delta = 0.2037$, respectively. The results are roughly proportional to $|\cos k_x - \cos k_y|$.

3.4 Density of states.

Figs. 4(a) and 4(b) show the calculated one-particle densities of states at $T = T_c$ (dashed lines) and $T = 0.0030$ (solid lines) for $\delta = 0.1451$ ($T_c = 0.0060$) and $\delta = 0.2037$ ($T_c = 0.0045$), respectively. It is seen in Fig. 4 that the pseudo-gap opens at $T = T_c$ due to the antiferromagnetic spin fluctuation. The superconducting gaps estimated from these figures are $2\Delta = 0.0663$ for $\delta = 0.1451$ ($2\Delta/k_B T_c = 11.0$) and $2\Delta = 0.0438$ for $\delta = 0.2037$ ($2\Delta/k_B T_c = 9.7$). The deviation of the frequency of the minimum density of state from the Fermi level at $T = 0.0030$ for $\delta = 0.2037$ seems to indicate that a size-effect still remains in the numerical work.

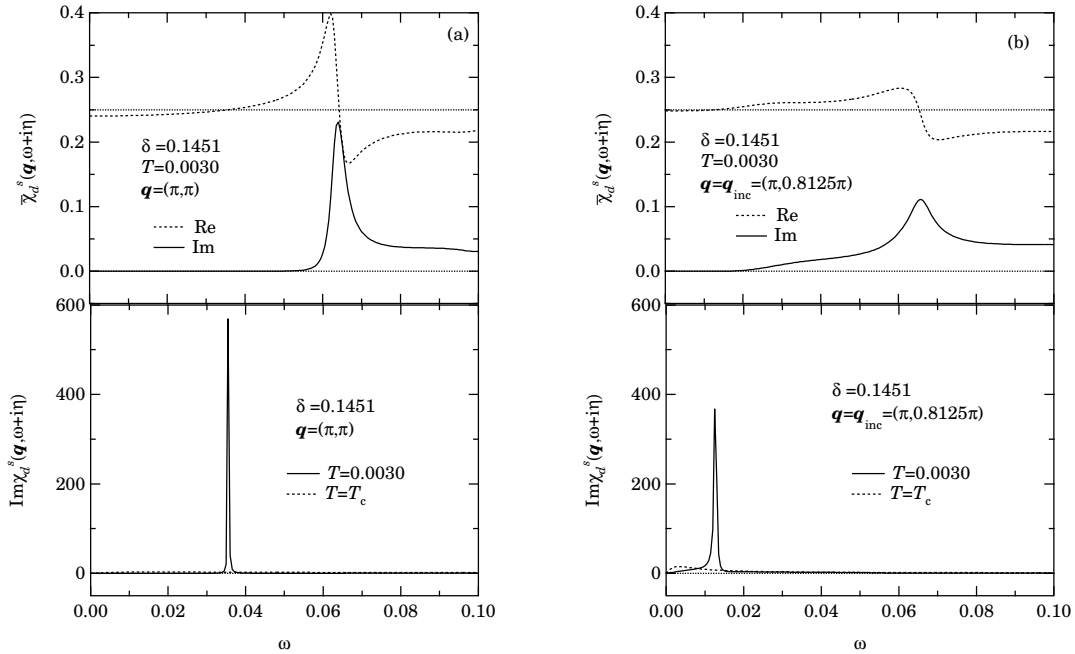


Fig. 5. Calculated dynamical susceptibilities; upper panels show the real and imaginary parts of the irreducible susceptibilities and the lower panels show the final results for $\delta = 0.1451$. (a) $\mathbf{q} = (\pi, \pi)$, (b) $\mathbf{q} = \mathbf{q}_{\text{inc}} = (\pi, 0.8125\pi)$.

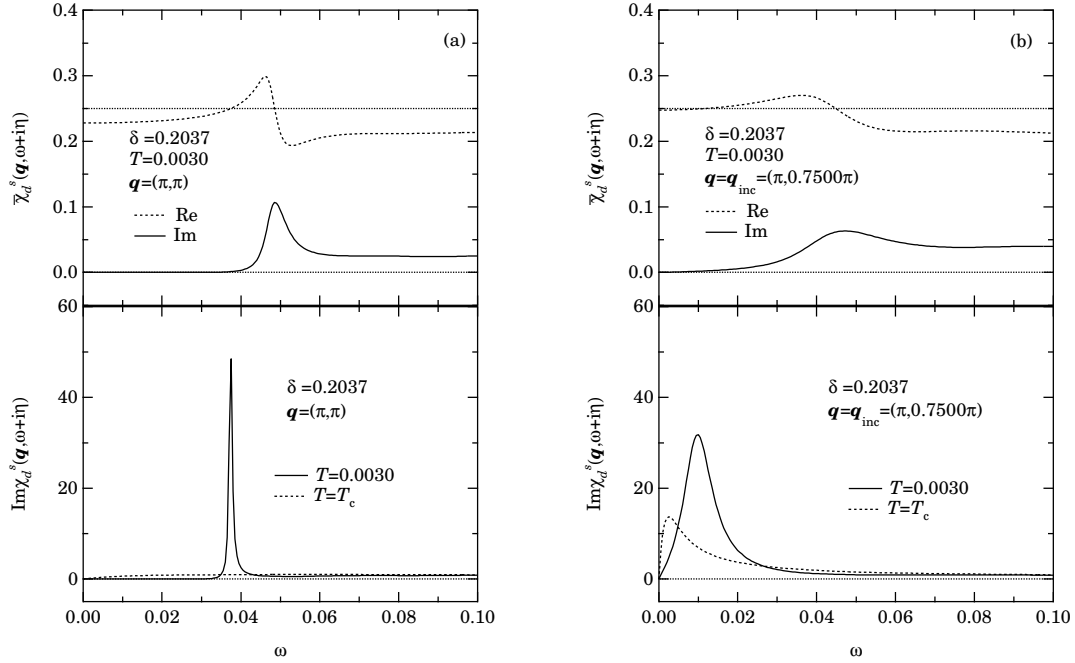


Fig. 6. Calculated dynamical susceptibilities; upper panels show the real and imaginary parts of the irreducible susceptibilities and the lower panels show the final results for $\delta = 0.2037$. (a) $\mathbf{q} = (\pi, \pi)$, (b) $\mathbf{q} = \mathbf{q}_{inc} = (\pi, 0.7500\pi)$.

3.5 Dynamical susceptibility.

We first show in Figs. 5(a) and 5(b) the ω -dependence of the dynamical susceptibility in the superconducting state for $\delta = 0.1451$ for the wave vectors $\mathbf{q} = \mathbf{Q} = (\pi, \pi)$ and $\mathbf{q} = \mathbf{q}_{inc}$, respectively, where \mathbf{q}_{inc} is the wave vector for the incommensurate peak of the susceptibility. The upper panels show the real and imaginary parts of the irreducible susceptibility $\bar{\chi}_d^s(\mathbf{q}, \omega + i\eta)$ and the lower panels show the imaginary part of $\chi_d^s(\mathbf{q}, \omega + i\eta)$. The results of the same calculation for $\delta = 0.2037$ are shown in Fig. 6. From these figures we find that $\text{Im}\bar{\chi}_d^s(\mathbf{q}, \omega + i\eta)$ has a peak at the value of $\omega = 2\Delta_{max}$ corresponding roughly to the energy gap in the density of states shown in Fig. 2: $2\Delta_{max} = 0.064$ for $\delta = 0.1451$ and $2\Delta_{max} = 0.049$ for $\delta = 0.2037$. On the other hand, $\text{Im}\chi_d^s(\mathbf{q}, \omega + i\eta)$ shows a sharp resonance peak at a frequency substantially smaller than $2\Delta_{max}$. This peak is considered to be specific to the superconducting state since it tends to vanish at T_c as may be seen in Figs. 5 and 6. From the same figures we may see that the resonance peaks grow at the expense of the lower frequency spin fluctuations in the normal state. Also, the peak intensity seems to be stronger when the energy gap is larger. The resonance nature of this peak may best be seen from the following expression:

$$\text{Im}\chi_d^s(\mathbf{q}, \omega + i\eta) = \frac{\text{Im}\bar{\chi}_d^s(\mathbf{q}, \omega + i\eta)}{[1 - U\text{Re}\bar{\chi}_d^s(\mathbf{q}, \omega + i\eta)]^2 + [U\text{Im}\bar{\chi}_d^s(\mathbf{q}, \omega + i\eta)]^2}. \quad (26)$$

and Figs. 5 and 6. In the denominator of the right hand side of this expression the second term may be quite small for the energies less than the superconducting gap energy. When the first term vanishes at $\omega = \omega_{\mathbf{q}}$, $\text{Im}\chi_d^s(\mathbf{q}, \omega + i\eta)$ naturally shows a sharp peak there. In Figs. 5 and 6 the resonance frequency $\omega_{\mathbf{q}}$ is given by the point where $\text{Re}\bar{\chi}_d^s(\mathbf{q}, \omega + i\eta)$ crosses the horizontal dotted lines indicating $1/U$. The peak width is given roughly by the magnitude of $\gamma_{\mathbf{q}} \equiv \text{Im}\bar{\chi}_d^s(\mathbf{q}, \omega_{\mathbf{q}} + i\eta)$. Figs. 7(a) and 7(b) show the calculated \mathbf{q} -dependences of $\omega_{\mathbf{q}}$ and $\gamma_{\mathbf{q}}$ for $\delta = 0.1451$ and $\delta = 0.2037$, respectively. It is interesting to note that $\omega_{\mathbf{q}} - \mathbf{q}$ curves are qualitatively similar to the corresponding results for the Hubbard model.[9]

Next we show in Figs. 8(a) and 8(b) the \mathbf{q} -integrated or local dynamical susceptibility $\text{Im}\chi(\omega)$ for $\delta = 0.1451$ and $\delta = 0.2037$, respectively. Here the solid and dashed lines show the results at $T = 0.0030$ and $T = T_c$, respectively.

Finally we note that the resonance peaks calculated here and the result of calculation for $\text{Im}\chi(\omega)$ bear striking resemblance to the results of neutron inelastic scattering experiments on $\text{YBa}_2\text{Cu}_3\text{O}_7$ [19, 20, 21, 22]

and $\text{YBa}_2\text{Cu}_3\text{O}_{6.5}$. [23] For more convincing comparisons, however, further experimental and theoretical studies are needed.

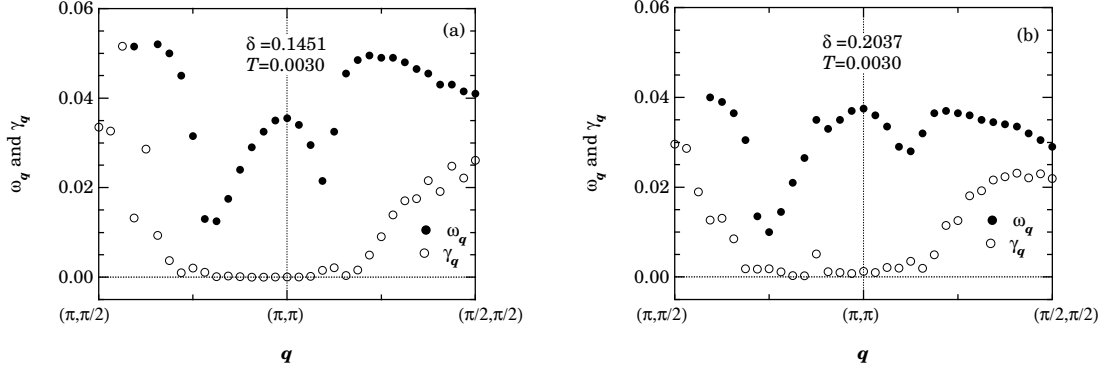


Fig. 7. The resonance peak positions of the dynamical susceptibility and the damping constant. (a) $\delta = 0.1451$, (b) $\delta = 0.2037$.

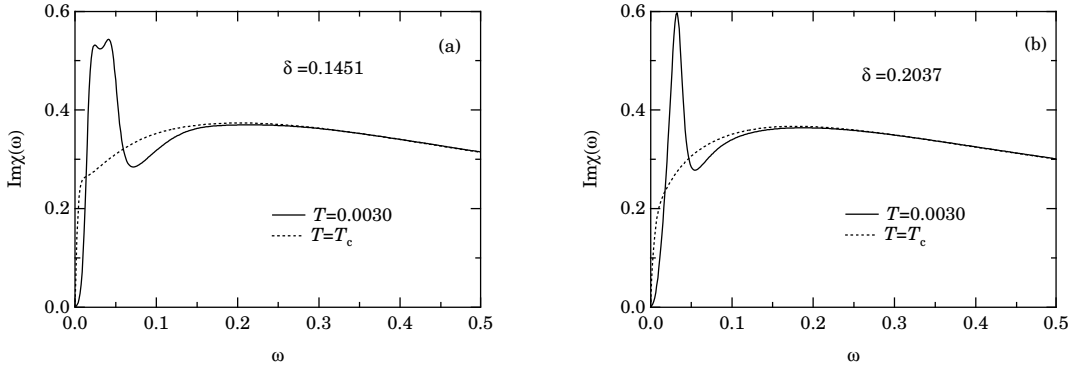


Fig. 8. Imaginary parts of the local or q -integrated dynamical susceptibility. (a) $\delta = 0.1451$, (b) $\delta = 0.2037$.

3.6 One electron spectral density.

We show in Fig. 9 the calculated one-particle spectral density $A(\mathbf{k}, \omega)$ for $\delta = 0.1451$ for five wave vectors around $\mathbf{k} = (\pi, 0)$, i.e., (a) $\mathbf{k} = (0.750\pi, 0)$, (b) $\mathbf{k} = (0.875\pi, 0)$, (c) $\mathbf{k} = (\pi, 0)$, (d) $\mathbf{k} = (\pi, 0.125\pi)$ and (e) $\mathbf{k} = (\pi, 0.250\pi)$, where the solid and dashed lines show the results for $T = 0.0030$ and $T = T_c$, respectively. Corresponding results for $\delta = 0.2037$ are shown in Fig. 10. From Figs. 9 and 10 we find a remarkable feature of $A(\mathbf{k}, \omega)$ in the superconducting state, consisting of a sharp coherent quasi-particle peak followed by a structure of dip and hump. As a matter of fact these behaviors are quite similar to those observed in the angle-resolved photoemission spectrum. [24, 25, 26, 27]

Next we show in Figs. 11(a) and 11(b) the dispersions of the coherent quasi-particle peaks and the humps together with the quasi-particle dispersion at $T = T_c$ around $\mathbf{k} = (\pi, 0)$ for $\delta = 0.1451$ and $\delta = 0.2037$, respectively. The dispersions are defined by the value of $\epsilon(\mathbf{k})$ giving a maximum value of $A(\mathbf{k}, \omega)$ for a given \mathbf{k} . These figures show that the quasi-particle peaks are almost dispersionless while the humps become indistinguishable from those in the normal state as we go away from the Fermi level. This behavior is also consistent with the results of ARPES measurements. [27]

In order to get better understanding of the above mentioned specific feature of the one-particle spectral density in the superconducting state, we show in Fig. 12 the calculated self-energy and the one-particle spectral

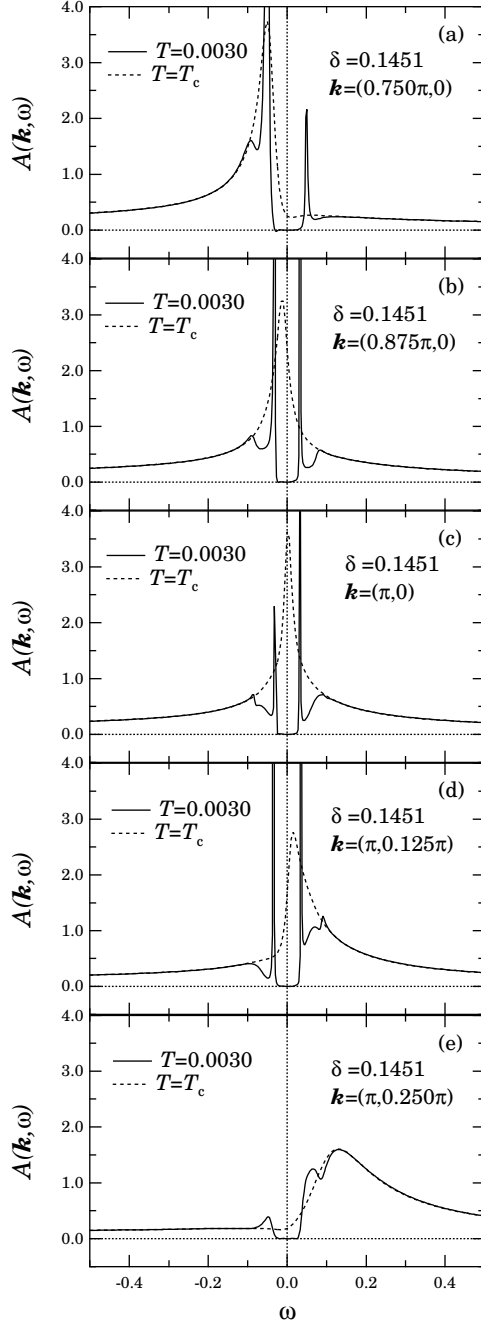


Fig. 9. One-electron spectral density around $\mathbf{k} = (\pi, 0)$ for $\delta = 0.1451$.

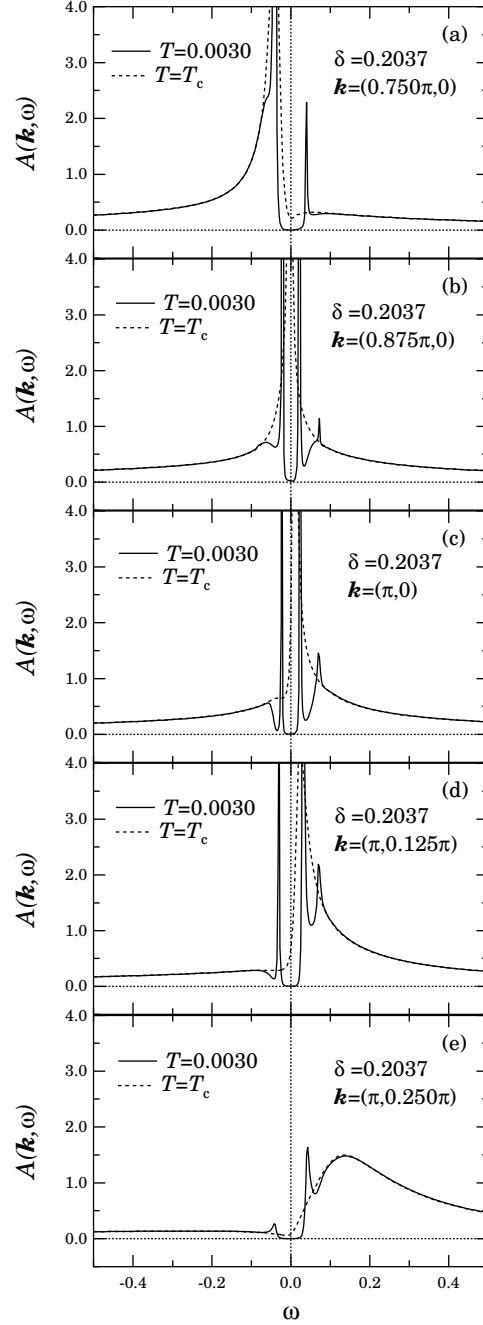


Fig. 10. One-electron spectral density around $\mathbf{k} = (\pi, 0)$ for $\delta = 0.2037$.

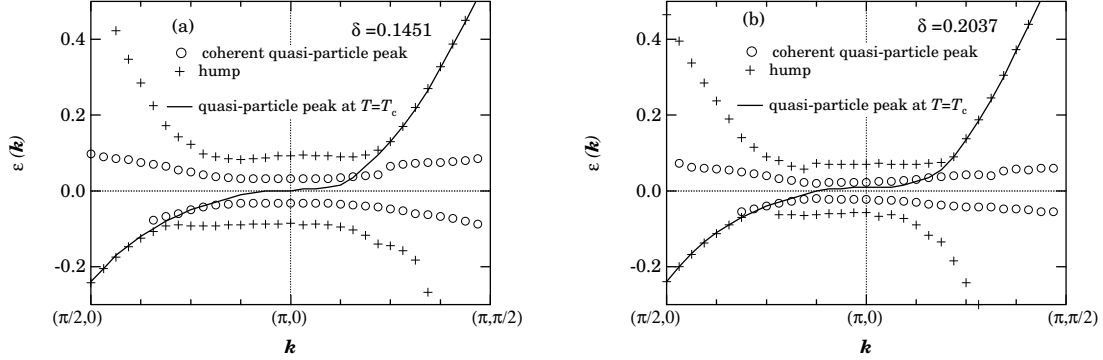


Fig. 11 Energy dispersions of the coherent quasi-particle peak and hump in the superconducting state ($T = 0.0030$). (a) $\delta = 0.1451$, (b) $\delta = 0.2037$.

density of the d -state, since the spectral density is dominated by this contribution. We have

$$\frac{1}{G_{dd}(\mathbf{k}, \omega + i\eta)} \equiv \frac{1}{G_{dd}^{(0)}(\mathbf{k}, \omega + i\eta)} - \Sigma(\mathbf{k}, \omega + i\eta), \quad (27)$$

$$A_d(\mathbf{k}, \omega) \equiv -\frac{1}{\pi} \text{Im}G_{dd}(\mathbf{k}, \omega + i\eta). \quad (28)$$

$$\Sigma(\mathbf{k}, \omega + i\eta) = \Sigma^{(1)}(\mathbf{k}, \omega + i\eta) - G_N^*(\mathbf{k}, -\omega + i\eta)[\Sigma^{(2)}(\mathbf{k}, \omega + i\eta)]^2, \quad (29)$$

$$\frac{1}{G_N(\mathbf{k}, \omega + i\eta)} \equiv \frac{1}{G_{dd}^{(0)}(\mathbf{k}, \omega + i\eta)} - \Sigma^{(1)}(\mathbf{k}, \omega + i\eta). \quad (30)$$

A quasi-particle peak is expected at the frequency which satisfies

$$\frac{1}{G_{dd}^{(0)}(\mathbf{k}, \omega + i\eta)} - \text{Re}\Sigma(\mathbf{k}, \omega + i\eta) = 0, \quad (31)$$

provided $\text{Im}\Sigma(\mathbf{k}, \omega + i\eta)$ is small at the same time. As is seen in Fig. 12 the superconducting energy gap gives almost vanishing values of $\text{Im}\Sigma(\mathbf{k}, \omega + i\eta)$ in a fairly wide frequency range around $\mathbf{k} = (\pi, 0)$ and sharp quasi-particle peaks are expected in this region of \mathbf{k} -space. As the frequency increases beyond this region $|\text{Im}\Sigma(\mathbf{k}, \omega + i\eta)|$ increases first rapidly and then gradually. At the same time the value of $[G_{dd}^{(0)}(\mathbf{k}, \omega + i\eta)]^{-1} - \text{Re}\Sigma(\mathbf{k}, \omega + i\eta)$ increases rapidly first to form a dip structure in $A_d(\mathbf{k}, \omega)$ and then the ω -dependence of this value reflect itself on the spectrum of $A_d(\mathbf{k}, \omega)$ as is expected from eqs. (27, 28) and is actually seen in Fig. 12.

4 Conclusion and Discussion

On the basis of the d - p model we have studied the unconventional superconducting state induced by the antiferromagnetic spin fluctuations in the optimal and over-doped regimes of high- T_c cuprates. Calculations were performed for the superconducting order parameter of $d_{x^2-y^2}$ symmetry, the dynamical susceptibility and the one-electron spectral density, by using the FLEX approximation, i.e., the strong coupling theory with the self-consistently renormalized random phase approximation (RRPA) for spin fluctuations. The order parameter or the gap function was found to develop more rapidly than in the BCS model, and the ratio of the low temperature maximum gap energy to $k_B T_c$ was about 10. The calculated spin fluctuation spectrum below T_c showed a resonance peak around $\mathbf{q} = (\pi, \pi)$ whose intensity was especially strong around the optimal doping concentration and its behavior bears striking resemblance to the peak at 41 meV observed in the neutron scattering experiment on $\text{YBa}_2\text{Cu}_3\text{O}_7$. The calculated one-particle spectral density showed a sharp

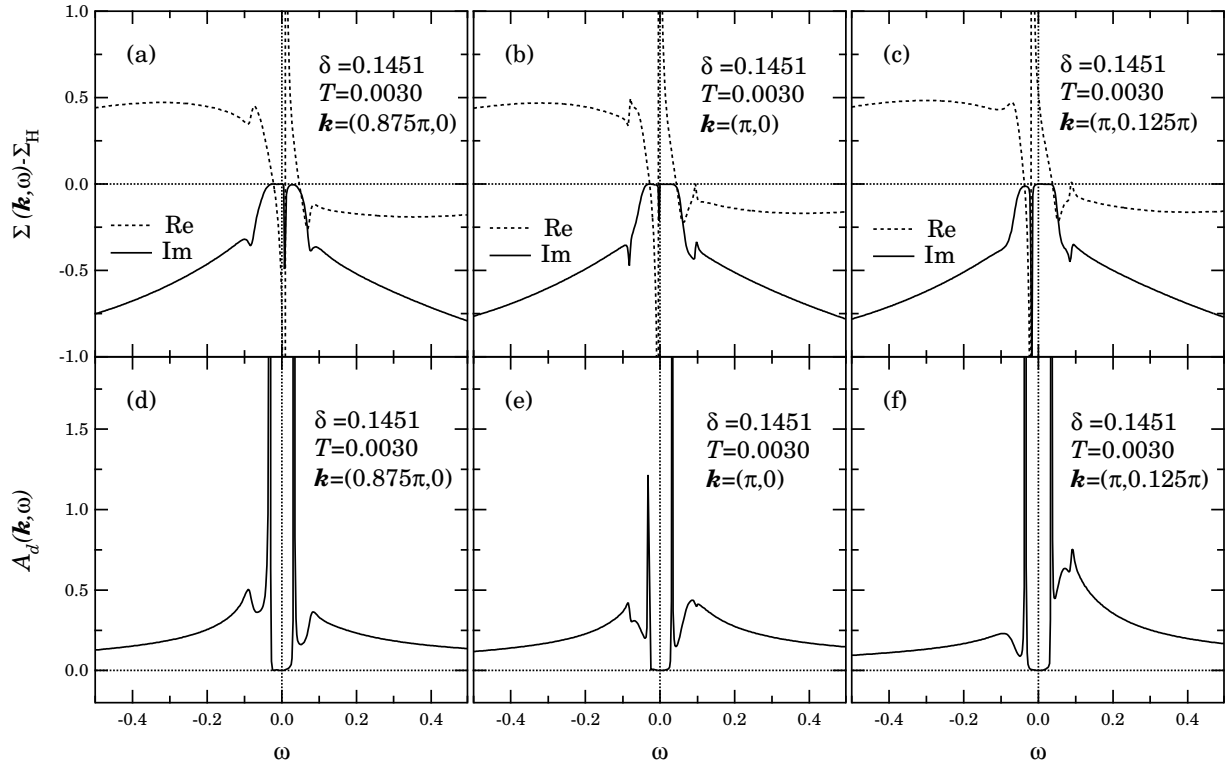


Fig. 12. Self-energy of the d -component of the Green's function and its one-particle spectral density at three points in the \mathbf{k} -space around $\mathbf{k} = (\pi, 0)$.

quasi-particle peak around $\mathbf{k} = (\pi, 0)$ followed by a structure with a dip and a hump. These results were quite similar to those observed in the ARPES spectra.

In view of these results we may conclude that the present calculation gives an additional support to the spin fluctuation mechanism for the high- T_c cuprates, especially in the optimal and over-doped concentration regimes.

Desired improvements of the present approach include the consideration of the vertex corrections neglected in the FLEX approximation. Although the effect was suggested to be insignificant or rather favorable for the superconductivity, [28] a self-consistent calculation with the vertex corrections is desired. The effect of impurity potential is expected to be more significant in the superconducting state than in the normal state. For example, the observed linear temperature dependences of $1/T_1$ and the specific heat far below T_c were successfully interpreted in terms of the additional density of states around the Fermi level caused by the impurity effect.[29] This effect will also have significant influence on the resonance peak in the dynamical susceptibility and on the above-discussed structures in the one-electron spectral density.

Of course there are many problems still to be clarified, particularly in the under-doped regime. The most controversial among them may be the pseudo-gap phenomena in the under-doped regime observed in NMR,[30] ARPES, [31, 32, 33, 34, 35] and other measurements. In the present approach we treat the spin fluctuations in the spirit of the self-consistent renormalization (SCR) theory which applies around the antiferromagnetic instability. However, the FLEX approximation without the vertex corrections may not be sufficient particularly in dealing with the low frequency phenomena. Also, it seems possible that the ground state in the under-doped regime has an antiferromagnetic long range order extending to the region rather far from the instability point. If such circumstances are really the case it seems necessary to develop an approximation beyond the conventional SCR, taking account of substantially larger effects of non-linear mode-mode couplings.

Acknowledgements

We are indebted Dr. S. Nakamura and Dr. H. Kondo for useful discussions particularly on numerical calculations.

References

- [1] T. Moriya, Y. Takahashi and K. Ueda: J. Phys. Soc. Jpn. **59** (1990) 2905; Physica C **185-189** (1991) 114.
- [2] K. Ueda, T. Moriya and Y. Takahashi: in *Electronic Properties and Mechanisms of High- T_c superconductors* (Tsukuba Symposium, 1991), eds. T. Oguchi, *et al.* (North Holland, Amsterdam, 1992) p. 145; J. Phys. Chem. Solids **53** (1992) 1515.
- [3] P. Monthoux, A. V. Balatsky and D. Pines: Phys. Rev. Lett. **67** (1991) 3448; Phys. Rev. B **46** (1992) 14803.
- [4] P. Monthoux and D. Pines: Phys. Rev. Lett. **69** (1992) 961; (E) **71** (1993) 208; Phys. Rev. B **47** (1993) 6069.
- [5] T. Moriya and K. Ueda: J. Phys. Soc. Jpn. **63** (1994) 1871.
- [6] P. Monthoux and D. Pines: Phys. Rev. B **49** (1994) 4261.
- [7] S. Nakamura, T. Moriya and K. Ueda: J. Phys. Soc. Jpn. **65** (1996) 4026.
- [8] N. E. Bickers, D. J. Scalapino and S. R. White: Phys. Rev. Lett. **62** (1989) 961; see also N. E. Bickers, D. J. Scalapino and R. T. Scalettar: Int. J. Mod. Phys. **B1** (1987) 687.
- [9] C.-H. Pao and N. E. Bickers: Phys. Rev. Lett. **72** (1994) 1870; Phys. Rev. B **51** (1995) 16310.
- [10] P. Monthoux and D. J. Scalapino: Phys. Rev. Lett. **72** (1994) 1874.
- [11] T. Dahm and L. Tewordt: Phys. Rev. B **52** (1995) 1297.
- [12] M. Langer, J. Schmalian, S. Grabowski and K. H. Bennemann: Phys. Rev. Lett. **75** (1995) 4508.
- [13] S. Grabowski, M. Langer, J. Schmalian and K. H. Bennemann: Europhys.Lett. **34** (1996) 219.
- [14] J. J. Deisz, D. W. Hess and J. W. Serene: Phys. Rev. Lett. **76** (1996) 1312.
- [15] R. Putz, R. Preuss, A. Muramatsu and W. Hanke: Phys. Rev. B **53** (1996) 5133.
- [16] G. Esirgen and N. E. Bickers: Phys. Rev. B **55** (1997) 2122; Phys. Rev. B **57** (1998) 5376.
- [17] S. Koikegami, S. Fujimoto and K. Yamada: J. Phys. Soc. Jpn. **66** (1997) 1438.
- [18] T. Takimoto and T. Moriya: J. Phys. Soc. Jpn. **66** (1997) 2459.
- [19] J. Rossat-Mignod, L. P. Regnault, C. Vettier, P. Bourges, P. Burlet, J. Bossy, J. Y. Henry and G. Lapertot: Physica C **185-189** (1991) 86.
- [20] H. A. Mook, M. Yethiraj, G. Aeppli, T. E. Mason and T. Armstrong: Phys. Rev. Lett. **70** (1993) 3490.
- [21] H. F. Fong, B. Keimer, P. W. Anderson, D. Reznik, F. Doğan and I. A. Aksay: Phys. Rev. Lett. **75** (1995) 316.
- [22] H. F. Fong, B. Keimer, D. L. Milius and I. A. Aksay: Phys. Rev. Lett. **78** (1997) 713.
- [23] P. Bourges, H. F. Fong, L. P. Regnault, J. Bossy, C. Vettier, D. L. Milius, I. A. Aksay and B. Keimer: Phys. Rev. B **56** (1997) R11439.

- [24] D. S. Dessau, B. O. Wells, Z.-X. Shen, W. E. Spicer, A. J. Arko, R. S. List, D. B. Mitzi and A. Kapitulnik: Phys. Rev. Lett. **66** (1991) 2160.
- [25] Z.-X. Shen and D. S. Dessau: Phys. Rep. **253** (1995) 1.
- [26] Z.-X. Shen and J. R. Schrieffer: Phys. Rev. Lett. **78** (1997) 1771.
- [27] M. R. Norman, H. Ding, J. C. Campuzano, T. Takeuchi, M. Randeria, T. Yokoya, T. Takahashi, T. Mochiku and K. Kadowaki: Phys. Rev. Lett. **79** (1997) 3506.
- [28] P. Monthoux: Phys. Rev. B **55** (1997) 15261.
- [29] T. Hotta: J. Phys. Soc. Jpn. **62** (1993) 274.
- [30] H. Yasuoka, T. Imai and T. Shimizu: in *Strong Correlation and Superconductivity*, eds. H. Fukuyama, S. Maekawa and A. P. Malozemoff. (Springer, Berlin, 1989) p. 254.
- [31] D. S. Marshall, D. S. Dessau, A. G. Loeser, C.-H. Park, A. Y. Matsuura, J. N. Eckstein, I. Bozovic, P. Fournier, A. Kapitulnik, W. E. Spicer and Z.-X. Shen: Phys. Rev. Lett. **76** (1996) 4841.
- [32] H. Ding, T. Yokoya, J. C. Campuzano, T. Takahashi, M. Randeria, M. R. Norman, T. Mochiku, K. Kadowaki and J. Giapintzakis: Nature **382** (1996) 51.
- [33] A. G. Loeser, Z.-X. Shen, D. S. Dessau, D. S. Marshall, C.-H. Park, P. Fournier and A. Kapitulnik: Science **273** (1996) 325.
- [34] M. R. Norman, H. Ding, M. Randeria, J. C. Campuzano, T. Yokoya, T. Takeuchi, T. Takahashi, T. Mochiku, K. Kadowaki, P. Guptasarma and D. G. Hinks: Nature **392** (1998) 157.
- [35] Z.-X. Shen, P. J. White, D. L. Feng, C. Kim, G. D. Gu, H. Ikeda, R. Yoshizaki and N. Koshizuka: Science **280** (1998) 259.